DOI: 10.1002/chem.201000390

Synthesis, Structure and Magnetic Phase Transitions of the Manganese Succinate Hybrid Framework, $Mn(C_4H_4O_4)$

Paul J. Saines,[a] Brent C. Melot,[b, c] Ram Seshadri,[b, c] and Anthony K. Cheetham*[a]

Abstract: An anhydrous manganese succinate, $Mn(C_4H_4O_4)$, has been synthesised hydrothermally and studied by single-crystal X-ray diffraction. It adopts a succinate pillared structure in which layers of corner-sharing MnO_6 octahedra alternate with sheets that contain chains of edge-sharing octahedra. This unique 3D framework structure contains highly distorted MnO_6 octahedra, which are made possible by the lack of ligand field stabilisation energy for the high-spin Mn^{2+} ion. Attempts to dope the structure with other divalent transition-metal ions were accordingly unsuccessful. Magnetic susceptibility and heat capacity measurements indicate that $Mn(C_4H_4O_4)$ undergoes antiferromagnetic ordering below 12 K, with a second antiferromagnetic transition at approximately 6 K. These two antiferromagnetic phases undergo further transitions in applied fields, underlining the subtle magnetic behaviour that is possible in inorganic–organic frameworks of this structural complexity.

Keywords: hybrid frameworks · magnetic properties · manganese · solid-state structures · X-ray diffraction

Introduction

The wide variety of fascinating properties found in inorganic–organic (hybrid) frameworks has led to them being the focus of extensive research.[1–3] Most of the attention has been lavished on nanoporous frameworks with bulky ligands and extensive metal–ligand–metal connectivity, commonly referred to as metal–organic frameworks (MOFs), many of which show excellent catalysis and gas-storage capabilities.[4] Recently, however, frameworks with extended inorganic (e.g., metal–oxygen–metal) connectivity have become of increasing interest.[2,5] These materials can exhibit the types of cooperative behaviour, such as ferromagnetism and electronic conductivity, which are commonly found in purely inorganic compounds, especially metal oxides. The structure-directing effects of the ligands on the framework, however, enable hybrids to adopt unusual structures with unique properties that are not found in inorganic compounds.

The divalent transition-metal succinates are a well-studied family of hybrid frameworks with extensive inorganic connectivity.[6–10] The metal–oxygen–metal bonding in these materials leads many of them to undergo magnetic ordering at medium to low temperatures.[7,9,11] The framework succinates are typically synthesised hydrothermally, and it has been found that the compositions, structures and extent of organic and inorganic connectivity of these materials, in particular the cobalt succinates, change significantly with the synthesis temperature.[10] To date, unlike the cobalt and nickel succinates, only one manganese succinate structure with any inorganic connectivity has been found.[7] This phase, $Mn_5(OH)_2(C_4H_4O_4)_4$, is isostructural with the high-temperature phase adopted by cobalt succinate. Given the diversity of the phases found with other divalent transition metals, and the range of stereochemistries that can be accommodated by the high-spin d^5 electron configuration of Mn^{2+}, it is interesting to examine whether there are any additional manganese succinate phases and what magnetic properties they might exhibit.

Herein we describe the synthesis and structural characterisation of an anhydrous manganese succinate with a new and apparently unique structure. It is unusual compared with other transition-metal succinates in that it consists of

[a] Dr. P. J. Saines, Prof. A. K. Cheetham
Department of Materials Science and Metallurgy
The University of Cambridge
Cambridge CB2 3QZ (UK)
Fax: (+44) 1223-334567
E-mail: akc30@cam.ac.uk

[b] B. C. Melot, Prof. R. Seshadri
Materials Department, University of California
Santa Barbara, California 93106 (USA)

[c] B. C. Melot, Prof. R. Seshadri
Department of Chemistry and Biochemistry
University of California, Santa Barbara, California 93106 (USA)

Supporting information for this article is available on the WWW under http://dx.doi.org/10.1002/chem.201000390.

layers of corner-sharing MnO_6 octahedra alternating with sheets in which the MnO_6 octahedra share edges. These layers are pillared by the succinate ligands. The complex magnetic properties of this remarkable compound are also described.

Results and Discussion

Structure of $Mn(C_4H_4O_4)$: $Mn(C_4H_4O_4)$ is the first octahedrally coordinated transition-metal succinate in which the cations are coordinated only by succinate ligands (see Table 1 for the crystallographic data). Most other transition-metal succinates have a mixture of aquo, hydroxy and succinate ligands, the only known exception being two tetrahedrally coordinated zinc succinates.[12] The asymmetric unit consists of two manganese cations, which are both on special positions, and one deprotonated succinate anion (see Figure 1). The two crystallographically distinct manganese cations are in alternating MnO_6 layers, which are interconnected along the *a* axis by the succinate ligands (see Figure 2a). The first of these layers has chains of edge-sharing MnO_6 octahedra, which run parallel to the *c* axis (Figure 2b). Chains within the same layer are cross-linked by carboxylate groups connecting this layer in an I^1O^1 fashion according to a two-dimensional modification of the notation of Cheetham et al.[1] The second layer consists of corner-sharing MnO_6 octahedra, which are connected along both the *b* and *c* axis (Figure 2c), giving this layer I^2O^0 connectivity. Each MnO_6 layer with the same connectivity is translated half the length of the unit cell along the *b* axis with respect to the analogous layer below, giving rise to a long *a* axis of 30.279(3) Å.

Table 1. Crystallographic data for manganese succinate $Mn(C_4H_4O_4)$.

	$Mn(C_4H_4O_4)$
formula	$MnC_4H_4O_4$
M_r	171.01
T [K]	120
crystal system	monoclinic
space group	*C*2/*c* (15)
a [Å]	30.279(3)
b [Å]	4.8583(4)
c [Å]	6.2910(6)
β [°]	99.550(3)
V [Å^3]	912.61(15)
Z	8
ρ_{calcd} [g cm^{-3}]	2.489
μ [cm^{-1}]	2.804
reflns measured/unique reflns	3943/1184 (R_{int} = 0.0533)
reflns refined	1038
parameters refined	68
R_1, wR_2[a] (all data)	0.0589, 0.1510
R_1, wR_2[a] (observed data)	0.0572, 0.1493

[a] $w = 1/[\sigma^2(F_o^2) + (aP)^2 + bP]$ and $P = (\max(F_o^2, 0) + 2F_c^2)/3$; $R_1 = \sum ||F_o| - |F_c|| / \sum |F_o|$ and $wR_2 = \sqrt{\{\sum [w(F_o^2 - F_c^2)^2] / \sum w(F_o^2)^2\}}$.

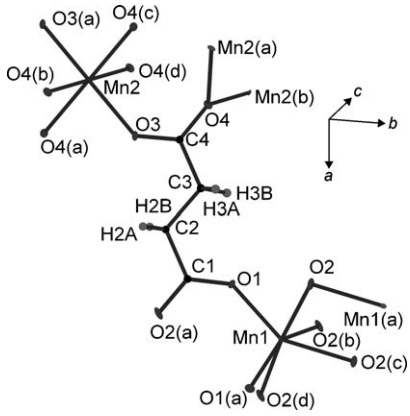

Figure 1. Asymmetric unit of $Mn(C_4H_4O_4)$ displayed with 80% probability displacement ellipsoids. Additional non-hydrogen atoms, included to illustrate the coordination sphere of each atomic position, are marked alphabetically.

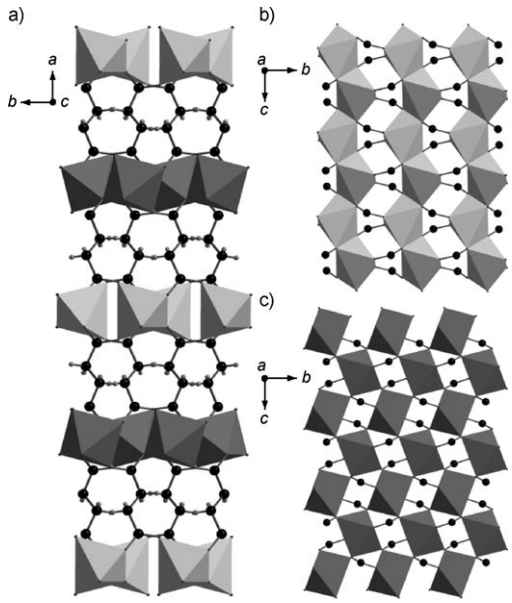

Figure 2. Ball-and-stick depictions of the 3D structure of $Mn(C_4H_4O_4)$: a) Side view of the two types of MnO_6 layers present in its structure viewed down the *c* axis; b) and c) The two different layers depicted in the *bc* plane (only atoms involved in intra-layer bonding are included). The layer in b shows the edge-sharing chains whereas c shows a corner-sharing MnO_6 sheet.

The bond valencies of the manganese in the edge- and corner-sharing layers are 2.03 and 1.93, respectively, confirming that the cations are divalent (see Table 2 for the Mn–O bond lengths and angles).[13] The manganese in the edge-sharing layer, Mn1, is bound to four O2 atoms and two O1 atoms. The O2 atoms occupy the adjacent corners of the edge-sharing MnO_6 octahedra and thus bond to two different Mn1 cations. The O1 oxygens are *cisoid* and only bond to one Mn cation, but they are involved in the organic connectivity along the *b* axis. In the corner-sharing MnO_6 layer, the manganese cation Mn2 is bound to four oxygen atoms on the O4 site, whereas the remaining two bonds are with

Table 2. Selected bond lengths [Å] and angles [°] in $Mn(C_4H_4O_4)$.

Bond	Bond length [Å] or angle [°]	Bond	Bond length [Å] or angle [°]
Mn1−O1	2×2.131(4)	Mn2−O3	2×2.080(4)
Mn1−O2	2×2.214(4)	Mn2−O4	2×2.243(4)
Mn1−O2	2×2.233(4)	Mn2−O4	2×2.364(4)
O1-Mn1-O1	109.5(2)	O3-Mn2-O3	180
O1-Mn1-O2	2×81.92(16)	O3-Mn2-O4	2×87.31(16)
O1-Mn1-O2	2×90.32(17)	O3-Mn2-O4	2×89.67(16)
O1-Mn1-O2	2×101.87(17)	O3-Mn2-O4	2×90.33(16)
O1-Mn1-O2	2×149.43(16)	O3-Mn2-O4	2×92.69(16)
O2-Mn1-O2	2×71.09(18)	O4-Mn2-O4	2×86.41(11)
O2-Mn1-O2	82.7(2)	O4-Mn2-O4	2×93.59(11)
O2-Mn1-O2	2×103.85(15)	O4-Mn2-O4	2×180
O2-Mn1-O2	173.5(2)		

oxygen atoms on the O3 site and are disposed in a *trans* fashion. Each oxygen atom on the O4 site forms bonds with two cations whereas the O3 oxygens only bond to one. Examination of the bond lengths of the corner-sharing octahedra (Mn2) shows that these are more varied than the edge-sharing octahedra (see Table 2). The bond angles of the edge-sharing octahedra (Mn1) are, however, substantially distorted from octahedral symmetry, unlike the corner-sharing octahedra. Therefore, both types of MnO_6 octahedra are severely distorted from regular octahedral symmetry, with the difference in the nature of the distortion most likely being related to constraints imposed by the different connectivities of the layers and the positions of the monodentate O1 and O3 atoms, which bond in the *cis* and *trans* positions in the edge- and corner-sharing layers, respectively.

The presence of alternating octahedrally coordinated metal–oxygen layers with such different geometries and connectivities is, in general, highly unusual and is unprecedented in succinate frameworks. The structure highlights the importance of the ligand in controlling the architecture of hybrid framework materials because, to the best of our knowledge, there are no directly analogous structures in purely inorganic metal oxides. An analogy with inorganic systems can, however, be drawn by viewing the different layers in the $Mn(C_4H_4O_4)$ structure as being analogous to those observed in the various derivatives of the perovskite structure.[14] Inorganic perovskite derivatives feature non-perovskite layers with a wide range of structures, including those found in the Ruddlesden–Popper phases, Aurivillius phases, hexagonal perovskites and the well-known $YBa_2Cu_3O_7$-type high-temperature superconducting cuprates.[14] We are, however, unaware of any perovskites that contain both edge- and corner-sharing octahedra in the same phase. Indeed, the Aurivillius phase Bi_2WO_6 appears to be the only known perovskite derivative that contains edge-sharing octahedra.[15] This occurs above 960 °C following a reconstructive transition in which the octahedra in the perovskite layer change from the corner-sharing motif adopted at lower temperatures to an edge-sharing arrangement. At no temperature does Bi_2WO_6 contain both corner- and edge-sharing octahedra in the same phase. Nevertheless, the wide variety of perovskite derivatives with different types of layers suggests that it is possible that such structural variety may also be found in inorganic–organic frameworks and further work should be done to explore this possibility.

Thermal analysis of $Mn(C_4H_4O_4)$: Thermogravimetric analysis indicates that $Mn(C_4H_4O_4)$ does not undergo significant mass loss below 290 °C, the temperature at which it decomposes (see Figure 1 in the Supporting Information). This confirms that, as indicated by the crystal structure and infrared spectroscopy, there is no solvent present in the structure. The compound loses 54.6 % mass between 290 and 360 °C, before a small mass gain to 46.2 % of the original weight in the range 450–620 °C. This is consistent with the complete decomposition of the ligand and the final formation of Mn_2O_3 in keeping with the brown colour of the final product (calcd 46.2 wt % of original). The small mass gain at higher temperatures is presumably related to the initial decomposition product being Mn_3O_4, which is oxidised to Mn_2O_3 on further heating.

Attempts to form solid solutions with $Mn(C_4H_4O_4)$: Samples of $Mn(C_4H_4O_4)$ synthesised in the presence of Fe^{2+}, Co^{2+} and Ni^{2+} were prepared to determine if it was possible to substitute different transition metals into this structure. Attempts to dope with Fe^{2+}, Co^{2+} and Ni^{2+} at temperatures between 100 and 200 °C failed to produce single-phase samples with the $Mn(C_4H_4O_4)$ structure, even with nominal dopant concentrations as low as 2.5 %. The $Mn(C_4H_4O_4)$ structure did, however, form as part of two-phase mixtures, most commonly with a $M_5(OH)_2(C_4H_4O_4)_4$ phase. The latter phase adopts $P2_1/c$ symmetry and is known to form for cobalt, iron and manganese succinates.[6,7,16] The lattice parameters of $Mn(C_4H_4O_4)$ remained unchanged in the two-phase mixtures, as determined by Rietveld refinement, suggesting that there is negligible solubility of other ions in this structure. This is in contrast to the $M_5(OH)_2(C_4H_4O_4)_4$ phase, and other phases that persist over a wide composition range at lower Mn^{2+} content, in which the lattice parameters contract with increasing Fe^{2+}, Co^{2+} and Ni^{2+} doping, as would be expected from the relative ionic radii of these ions (compare the ionic radius of 0.830 Å for high-spin Mn^{2+} to 0.690, 0.745 and 0.780 Å for Ni^{2+}, high-spin Co^{2+} and Fe^{2+}).[17] The inability to dope significant concentrations of Fe^{2+}, Co^{2+} and Ni^{2+} into $Mn(C_4H_4O_4)$ suggests that the compound owes its stability to the flexibility of the d^5 electronic configuration of Mn^{2+}. This configuration allows Mn^{2+} cations to adopt a variety of stereochemistries, including the more distorted octahedral geometries found in the title compound. These geometries are unfavourable for cations with significant ligand field stabilisation energies.

Magnetic properties of $Mn(C_4H_4O_4)$: The magnetic susceptibility measurements on $Mn(C_4H_4O_4)$ reveal antiferromagnetic ordering below 12 K (see Figure 3a). Above this temperature the compound exhibits Curie–Weiss paramagnetism, with fits to $1/\chi$ obtained in a 10 kOe field yielding a Curie–Weiss theta of −17 K and a magnetic moment, μ_{eff}, of

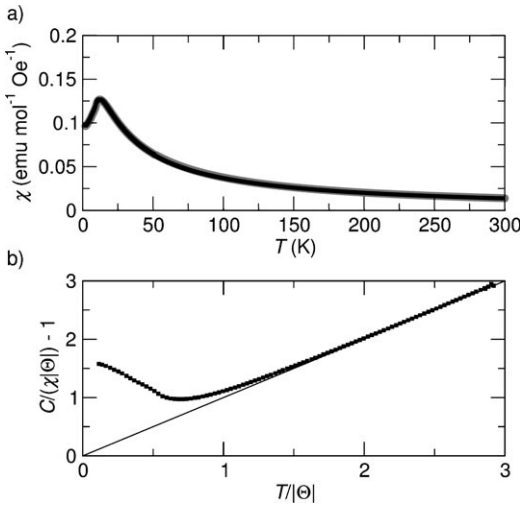

Figure 3. Plot of a) the magnetic susceptibility of $Mn(C_4H_4O_4)$ over the range of 2 K to 300 K (ZFC (●) and FC (■)) and b) $C/(\chi|\Theta|) - 1$ versus $T/|\Theta|$ in a 10 kOe applied field.

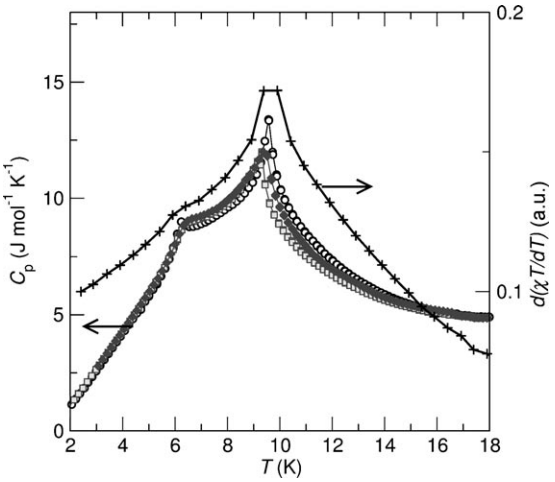

Figure 4. Heat capacity measurements for $Mn(C_4H_4O_4)$ measured in 0 (○), 25 (□) and 30 kOe (◈) applied fields and the Fisher heat capacity determined by using magnetic susceptibility data collected at 100 Oe (+).

5.91 μ_B per Mn^{2+}, which is very close to the expected spin-only moment of 5.92 μ_B. A plot of $C/(\chi|\Theta|) - 1$ as a function of $T/|\Theta|$(in which C = the Curie constant, χ = the magnetic susceptibility, and Θ is the Curie–Weiss theta) provides insight into the nature of the magnetic exchange interactions above the ordering temperature and gives an indication of the degree of magnetic frustration.[18] The plot shows a positive deviation from the ideal Curie–Weiss law very near to the Curie–Weiss temperature, indicating that the title compound has purely compensated antiferromagnetic interactions with little or no magnetic frustration (Figure 3b). The zero-field-cooled (ZFC) and field-cooled (FC) curves, obtained under fields of 100 and 10 kOe, respectively, are almost coincident down to the lowest temperature measured (see Figure 3a). The ac magnetic susceptibility measurements measured over a range of 1 to 1000 Hz (not shown) reveal no frequency dependence to the ordering peak, confirming that the spins are rigidly ordered and there is no glassiness or magnetic frustration present.

Heat capacity measurements, however, show that the magnetic behaviour of the system is more complex than Figure 3 would suggest. In particular, the heat capacity, C_p, which was studied as function of temperature at fields of 0, 25 and 30 kOe, shows two discontinuities at 6 and 10 K (Figure 4). The 10 K transition is clearly associated with the onset of magnetic order and is depressed slightly in temperature with increasing field strength.

Fisher has shown that the heat capacity of an antiferromagnet can be determined from the magnetic susceptibility by using the equation $C_{(T)} = A(\partial(\chi T)/\partial T)$, in which A is a constant that slowly varies as a function of T.[19] As can be seen for the 100 Oe field-cooled magnetic susceptibility data in Figure 4, a plot of the Fisher heat capacity reveals both of the features found in the conventional heat capacity data, although the discontinuity at 6 K is very small. Because the upturn of the heat capacity curves in fields of 25 and 30 kOe occurs at approximately the same temperature, this 6 K transition clearly persists in higher applied fields.

The isothermal magnetization loop, collected at 2 K, shows no sign of hysteresis and only reaches an induced magnetisation of 1.2 μ_B per Mn^{2+} by 50 kOe (Figure 5a). The magnetization loops reveal a non-linear dependence on the applied field, which is most likely due to the presence of multiple magnetic-field-induced transitions. By taking the derivative of the magnetization loop, two discontinuities are found at 22 and 27 kOe (Figure 5b). Magnetic susceptibility data obtained in applied fields of 25 and 30 kOe indicate a flattening out or slight upturn in the susceptibility around 7 K, which is not observed in weaker fields (Figure 6). The ZFC and FC curves collected at 25 and 30 kOe are still coincident below the ordering temperature, which suggests that these magnetic phases remain well ordered. These suscepti-

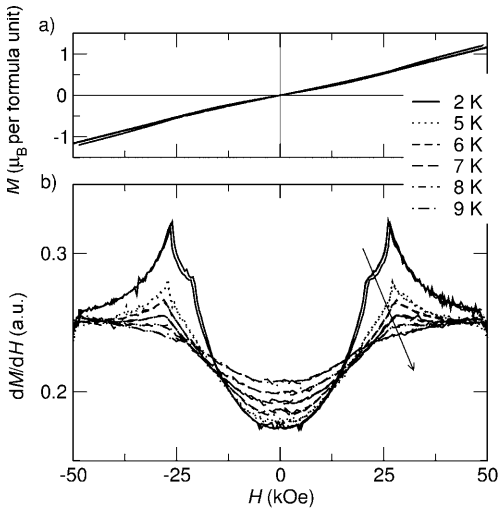

Figure 5. Plot of a) the isothermal magnetisation and b) the derivative of the magnetisation measured at 2 to 9 K for $Mn(C_4H_4O_4)$.

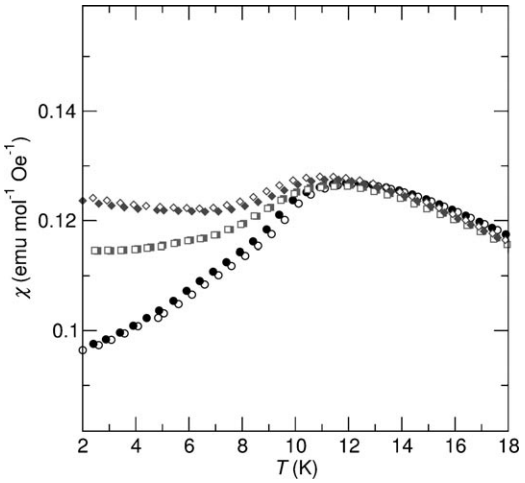

Figure 6. Plot of magnetic susceptibility of $Mn(C_4H_4O_4)$ in applied fields of 100 Oe (●), 25 (■) and 30 kOe (◆). Open and filled symbols represent susceptibility measured from zero-field cooled and field-cooled studies, respectively.

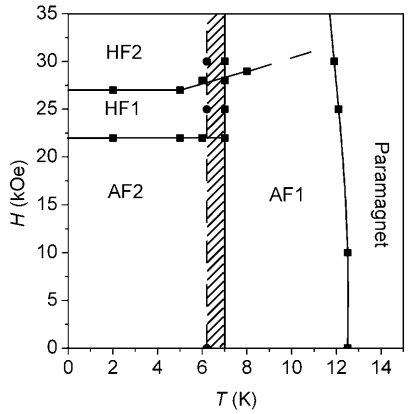

Figure 7. Phase diagram of magnetic transitions in $Mn(C_4H_4O_4)$ with the antiferromagnetic and high-field phases being denoted as AF and HF, respectively. Phase-transition temperatures determined by magnetic measurements (—— and ■) and transition temperatures determined by heat capacity measurements (– – – and ●). The hatched region between 6 and 7 K indicates the discrepancy between the temperature of the phase transition from the high-temperature antiferromagnetic phase to lower temperature phases as determined by magnetic and heat capacity measurements.

bility measurements also suggest that the ordering transition at 12 K is depressed slightly with increasing applied field, consistent with heat capacity measurements.

Isothermal magnetization loops were collected between 5 and 9 K to determine how the magnetic phase near the 6 K transition is affected by increasing the applied field (see Figure 5b). There is no clear indication of the transition observed at 22 kOe occurring above 7 K. The loops also indicate that the magnetic transition observed at 27 kOe occurs up to 8 K, although the field strength at which it occurs increases slightly to around 29 kOe. The discontinuity in the derivative of the magnetic loops at 7 K and 8 K is, however, much broader than is observed for lower temperatures.

Certain general conclusions can be drawn concerning the magnetic behaviour of the title compound: 1) There are clearly two magnetic phases in the low-field data, one that orders at approximately 10 K and a second that forms at approximately 6 K; 2) these phases appear to be antiferromagnetic and will be referred to as AF1 and AF2, respectively; 3) the lower temperature phase, AF2, undergoes two magnetic transitions on increasing the applied field, the first at approximately 22 kOe and the second at approximately 27 kOe; 4) the second of these magnetic transitions is observed above 6 K when AF1 is studied in an applied field, but the situation with the lower field transition is less clear. These conclusions are summarised in a tentative, magnetic phase diagram shown in Figure 7. It is tempting to speculate that the complex behaviour must be related to the different types of inorganic layers shown in Figure 2b and c, but there are clearly a number of possibilities that cannot be differentiated without further information. For example, AF1 and AF2 may be associated with ordering within the two different layer types, which then undergo further transitions in applied fields. Alternatively, we may be dealing with a spin-reorientation transition on going from AF1 to AF2. Such transitions have been seen in other high-spin d^5 systems such as Fe_2O_3 and $FePO_4$.[20] We intend to carry out a neutron diffraction study of $Mn(C_4D_4O_4)$ to evaluate the different possibilities and elucidate the precise magnetic structure of this framework.

$Mn(C_4H_4O_4)$ is the first Mn succinate to feature strongly ordered magnetic behaviour because $Mn_5(OH)_2(C_4H_4O_4)_4$, the only previous Mn succinate known to exhibit magnetic order, is highly frustrated and only exhibits weak antiferromagnetic behaviour.[7] The temperature at which $Mn(C_4H_4O_4)$ orders is similar to the manganese glutarate $Mn(CO_2(CH_2)_3CO_2)(H_2O)$, which also has extensive inorganic connectivity within layers and orders ferrimagnetically at 7 K.[21] Both compounds order at slightly higher temperatures than the organically bridged manganese malate, malonate and tartrate frameworks, which order antiferromagnetically or ferrimagnetically at around 4 K.[22] This highlights the importance of inorganic connectivity in raising the magnetic ordering temperature in metal–organic frameworks because of the shorter M–O–M distances and lower number of non-magnetic atoms between metal centres.

Conclusion

The anhydrous Mn succinate framework, $Mn(C_4H_4O_4)$, has been synthesised for the first time. It was found to adopt a unique structure containing alternating sheets of edge-sharing MnO_6 octahedral chains and layers of corner-sharing MnO_6 octahedra. The Mn^{2+} bonding environments in both layers are significantly distorted from regular octahedral geometry, albeit in significantly different ways. Coupled with the inability to dope other transition metals into the framework, this suggests that the Mn^{2+} cation's lack of ligand field stabilisation energy and, therefore, its ability to adopt

distorted bonding environments is crucial in stabilising this unusual structure.

Magnetic susceptibility and heat capacity data indicate that the title compound is antiferromagnetically ordered below 12 K with a second transition at approximately 6 K. The lowest temperature antiferromagnetic phase was found to undergo two field-induced magnetic phase transitions at approximately 22 and 27 kOe, which appear to result in an increase in the magnetic susceptibility. The higher field transition persists in the high-temperature antiferromagnetic phase although the situation with the lower field transition is unclear. The four magnetic phases all appear to be well ordered with no indication of magnetic frustration or glassiness. The complex magnetic behaviour of this compound is provisionally described in a phase diagram. Although the precise nature of these phases has not been established the subtle magnetic behaviour of $Mn(C_4H_4O_4)$ underlines the fascinating possibilities for inorganic–organic frameworks of this structural complexity.

Experimental Section

General methods and materials: Hydrothermal methods were used to synthesise all the samples examined in this work. Initially, light-pink sheet-shaped crystals of the title compound were obtained from a mixture of $MnCl_2{\cdot}4H_2O$, succinic acid, KOH and water in a 1:1.5:2.5:200 molar ratio with a total of 9 mL of water. This mixture was placed in a 23 mL teflon-lined Parr autoclave and then heated at 180 °C for 40 h. Phase-pure powder samples were synthesised from similar mixtures, but in those cases a molar ratio of 1:1.5:2.5:100 was used. It was found that $Mn(C_4H_4O_4)$ could be synthesised in a phase-pure form over a large temperature range, 100–200 °C, and by heating the autoclaves for either 40 or 90 h. The powder samples used in the characterisation of this compound were synthesised by heating for 90 h at either 180 or 200 °C. Doped samples were synthesised by using the same concentrations as the manganese samples (but with mixtures of $MnCl_2{\cdot}4H_2O$ plus $FeCl_2{\cdot}4H_2O$, $CoCl_2{\cdot}6H_2O$ or $NiCl_2{\cdot}6H_2O$), heating at temperatures between 100 °C and 200 °C. Infra-red spectra were collected over the range of 4000–500 cm^{-1} on a Bruker Tensor-27 ATR spectrometer. Elemental analysis of bulk $Mn(C_4H_4O_4)$ was obtained at the Department of Chemistry, the University of Cambridge (UK). Thermogravimetric analysis (TGA) was performed in air on a TA instruments Q50 using a heating rate of 10 °C $minute^{-1}$. The temperature dependence of the dc magnetization was measured on well-ground powder samples by using a Quantum Design MPMS 5XL SQUID magnetometer. Powder was preferred because a crystal of sufficient shape and dimensions could not be prepared. The specific heat data were collected by using the semi-adiabatic technique, as implemented in a Quantum Design Physical Property Measurement System (PPMS). $Mn(C_4H_4O_4)$ was mixed with equal parts by mass of Ag powder and pressed into a pellet to improve thermal coupling. The contribution from Ag was measured separately and subtracted.

Characterisation of $Mn(C_4H_4O_4)$: IR (ATR): $\tilde{\nu}$ = 1578, 1548, 1445, 1412, 1385 and 1215 cm^{-1} associated with stretching features of the carboxylate anion, $\nu(CO_2^-)$ and ν(C–O), $\tilde{\nu}$ = 1172 cm^{-1} associated with ν_{as}(C–C), $\tilde{\nu}$ = 931, 837, 806, 657, 595 and 594 cm^{-1} associated with metal–oxygen bonding and ν(C–H);[16,23] elemental analysis calcd (%) for $MnC_4H_4O_4$: C 28.09 H 2.36; found: C 28.08 H 2.33.

X-ray crystallography: Single-crystal X-ray diffraction data were collected at 120 K on a Bruker-Nonius Kappa diffractometer equipped with a Bruker Apex II CCD detector using X-rays from a Bruker-Nonius FR591 rotating anode X-ray generator ($Mo_{K\alpha}$ radiation, λ = 0.71073 Å). Data were collected over the range 2.91 to 27.48° (2θ) by using a plate-like crystal (0.18 × 0.11 × 0.01 mm^3) that was non-merohedrally twinned about the direct axis 00$\bar{1}$. The structure was solved in space group *C*2/*c* by Patterson synthesis by using DIRDIF 2008[24] and subsequently refined against $|F|^2$ by using SHELX-97[25] (see Table 1 for a summary of the crystal data) through the WinGX interface.[26] Absorption corrections were carried out by using SADABS.[27] An extinction parameter was not refined for the final cycles because it was determined, by using SHELX-97, to be within one estimated standard deviation (esd) of zero. Hydrogen atoms were geometrically constrained by using the AFIX commands in SHELX-97 and their thermal parameters were fixed to be 1.2 times those of the carbon atoms to which they are attached, but the C–H bond lengths were allowed to vary. Mn and O displacement parameters were refined anisotropically. C displacement parameters were refined isotropically because anisotropic refinement led to two of the carbons being non-positive definite. Even when refined anisotropically, however, the C displacement parameters were within two esds of their isotropic value and did not increase the quality of the refinement significantly (χ^2 and R_1 of 1.26 and 5.8% compared with 1.27 and 5.9%). CCDC-765956 contains the supplementary crystallographic data for this paper. These data can be obtained free of charge from The Cambridge Crystallographic Data Centre via www.ccdc.cam.ac.uk/data_request/cif.

Powder X-ray diffraction data were collected over the range of 5 to 60° (2θ) on a Bruker D8 Advance diffractometer using a linear position detector with $Cu_{K\alpha}$ radiation. These data were used to establish the bulk-phase composition and purity and, where necessary, a Rietveld refinement carried out by using the program Rietica,[28] was used to determine the lattice parameters.

Acknowledgements

The authors thank the EPSRC National Crystallographic Service for obtaining single-crystal data used in this study. P.J.S. and A.K.C. also acknowledge the University of Cambridge and the European Research Council for providing financial support. B.C.M. and R.S. thank the National Science Foundation for support through a Career Award (NSF-DMR 0449354) and for the use of MRSEC facilities (Award NSF-DMR 0520415).

[1] A. K. Cheetham, C. N. R. Rao, R. K. Feller, *Chem. Commun.* **2006**, 4780–4795.
[2] C. N. R. Rao, A. K. Cheetham, A. Thirumurugan, *J. Phys. Condens. Matter* **2008**, *20*, 083202.
[3] J. R. Long, O. M. Yaghi, *Chem. Soc. Rev.* **2009**, *38*, 1213–1214.
[4] a) A. U. Czaja, N. Trukhan, U. Müller, *Chem. Soc. Rev.* **2009**, *38*, 1284–1293; b) J. Lee, O. K. Farha, J. Roberts, K. A. Scheidt, S. T. Nguyen, J. T. Hupp, *Chem. Soc. Rev.* **2009**, *38*, 1450–1459; c) L. J. Murray, M. Dincă, J. R. Long, *Chem. Soc. Rev.* **2009**, *38*, 1294–1314.
[5] M. Kurmoo, *Chem. Soc. Rev.* **2009**, *38*, 1353–1379.
[6] Y. Kim, D.-Y. Jung, *Bull. Korean Chem. Soc.* **1999**, *20*, 827–830.
[7] Y. Kim, D.-Y. Jung, K.-P. Hong, G. Demazeau, *Solid State Sci.* **2001**, *3*, 837–846.
[8] a) P. M. Forster, A. K. Cheetham, *Angew. Chem.* **2002**, *114*, 475–477; *Angew. Chem. Int. Ed.* **2002**, *41*, 457–459; b) N. Guillou, C. Livage, G. Férey, *Eur. J. Inorg. Chem.* **2006**, 4963–4978.
[9] N. Guillou, C. Livage, W. van Beek, M. Noguès, G. Férey, *Angew. Chem.* **2003**, *115*, 667–671; *Angew. Chem. Int. Ed.* **2003**, *42*, 643–647.
[10] a) P. M. Forster, A. R. Burbank, C. Livage, G. Férey, A. K. Cheetham, *Chem. Commun.* **2004**, 368–369; b) P. M. Forster, N. Stock, A. K. Cheetham, *Angew. Chem.* **2005**, *117*, 7780–7784; *Angew. Chem. Int. Ed.* **2005**, *44*, 7608–7611.
[11] a) C. Livage, C. Egger, G. Férey, *Chem. Mater.* **1999**, *11*, 1546–1550; b) L.-S. Long, X.-M. Chen, M.-L. Tong, Z.-G. Sun, Y.-P. Ren, R.-B. Huang, L.-S. Zheng, *Dalton Trans.* **2001**, 2888–2890; c) D. Ghoshal, A. K. Ghosh, G. Mostafa, J. Ribas, N. R. Chaudhuri, *Inorg. Chim. Acta* **2007**, *360*, 1771–1775.

[12] T. A. Bowden, H. L. Milton, A. M. Z. Slawin, P. Lightfoot, *Dalton Trans.* **2003**, 936–939.
[13] a) I. D. Brown, D. Altermatt, *Acta Crystallogr. Sect. B* **1985**, *41*, 244–247; b) N. E. Brese, M. O'Keeffe, *Acta Crystallogr. Sect. B* **1991**, *47*, 192–197.
[14] R. H. Mitchell, *Perovskites Modern and Ancient*, Almaz Press, Ontario, **2002**.
[15] N. A. McDowell, K. S. Knight, P. Lightfoot, *Chem. Eur. J.* **2006**, *12*, 1493–1499.
[16] C. Livage, C. Egger, G. Férey, *Chem. Mater.* **2001**, *13*, 410–414.
[17] R. D. Shannon, *Acta Crystallogr. Sect. A* **1976**, *32*, 751–767.
[18] B. C. Melot, J. E. Drewes, R. Seshadri, E. M. Stoudenmire, A. P. Ramirez, *J. Phys. Condens. Matter* **2009**, *21*, 216007.
[19] a) M. E. Fisher, *Proc. R. Soc. London Ser. A* **1960**, *254*, 66–85; b) B. Cage, P. Nguyen, N. Dalal, *Solid State Commun.* **2001**, *119*, 597–601.
[20] a) F. J. Morin, *Phys. Rev.* **1950**, *78*, 819–820; b) C. G. Shull, W. A. Strauser, E. O. Wollan, *Phys. Rev.* **1951**, *83*, 333–345; c) I. Dzyaloshinsky, *J. Phys. Chem. Solids* **1958**, *4*, 241–255; d) P. D. Battle, A. K. Cheetham, C. Gleitzer, W. T. A. Harrison, G. J. Long, G. Longworth, *J. Phys. C* **1982**, *15*, L919–924.
[21] Y. Kim, Y. Park, D.-Y. Jung, *Inorg. Chem. Commun.* **2004**, *7*, 347–349.
[22] a) T. K. Maji, S. Sain, G. Mostafa, T.-H. Lu, J. Ribas, M. Monfort, N. R. Chaudhuri, *Inorg. Chem.* **2003**, *42*, 709–716; b) A. Beghidja, P. Rabu, G. Rogez, R. Welter, *Chem. Eur. J.* **2006**, *12*, 7627–7638; c) E. Coronado, J. R. Galàn-Mascarós, C. J. Gómez-García, A. Murcia-Martínez, *Chem. Eur. J.* **2006**, *12*, 3484–3492.
[23] K. D. Dobsonson, A. J. McQuillan, *Spectrochim. Acta Part A* **1999**, *55*, 1395–1405.
[24] P. T. Beurskens, G. Beurskens, R. de Gelder, S. Garcia-Granda, R. O. Gould, J. M. M. Smits, *The DIRDIF2008 Program System*, Crystallography Laboratory, University of Nijmegen, Nijmegen, **2008**.
[25] G. M. Sheldrick, *Acta Crystallogr. Sect. A* **2008**, *64*, 112–122.
[26] L. J. Farrugia, *A Windows Program for Crystal Structure Analysis*, University of Glasgow, Glasgow, **1998**.
[27] G. M. Sheldrick, SADABS, 2007/2, Bruker AXS Inc., Madison, Wisconsin, **2007**.
[28] B. A. Hunter, C. J. Howard, *A Computer Program for Rietveld Analysis of X-ray and Neutron Powder Diffraction Patterns*, Lucas Heights Laboratories, **1998**.

Received: February 12, 2010
Published online: May 19, 2010

